crystals

MDPI

Article

Correlation between Mechanical Properties—Structural Characteristics and Cavitation Resistance of Cast Aluminum Alloy Type 5083

Dionisie Istrate [1], Beatrice-Gabriela Sbârcea [2,*], Alin Mihai Demian [1], Andreea Daniela Buzatu [1], Laura Salcianu [3], Ilare Bordeasu [3,*], Lavinia Madalina Micu [4], Cristian Ghera [3], Bogdan Florea [5] and Brândușa Ghiban [1,*]

1 Metallic Materials Science and Physical Metallurgy Department, University Politehnica of Bucharest, 313 Splaiul Independentei, 060042 Bucharest, Romania
2 Department of Materials and Products Characterization for Electrical and Energy Engineering, National Institute for R&D in Electrical Engineering ICPE-CA, 313 Splaiul Unirii, 030138 Bucharest, Romania
3 Department of Mechanical Machines Equipment and Transportation, University Politehnica of Timisoara, 2 Piata Victoriei, 300006 Timisoara, Romania
4 Department of Agricultural Technologies, University of Agricultural Sciences and Veterinary Medicine of Banat King Mihai I from Romania, 119 Calea Aradului, 300645 Timisoara, Romania
5 Engineering and Management of Obtaining Metallic Materials Department, University Politehnica of Bucharest, 313 Splaiul Independentei, 060042 Bucharest, Romania
* Correspondence: gabriela.sbarcea@icpe-ca.ro (B.-G.S.); ilarica59@gmail.com (I.B.); ghibanbrandusa@yahoo.com (B.G.)

Abstract: The aluminum alloy type 5083, which has high corrosion resistance, excellent weldability, and good strength, is widely used in shipbuilding, automotive, aerospace, and industrial construction. The present paper has the aim of establishing a possible correlation between mechanical properties, structural characteristics, and cavitation erosion properties of the 5083 alloy after applying different heat treatments. Different homogenization heat treatments (350 °C, 450 °C) were applied, each followed by cooling in air and artificial aging at different temperature (140 °C and 180 °C) with three maintenance periods, 1 h, 12 h, and 24 h. The experiments concerning cavitation resistance of the experimental samples were completed in accordance with ASTM G32-2016. The cavitation erosion resistance were determined either by analytical diagrams MDER (or MDE) vs. cavity attack duration, or by measuring the maximum erosion attack by stereomicroscopy and scanning electron microscopy. Finally, the best combination of heat treatments applied to cast aluminum products type 5083 is homogenization at 350 °C followed by artificial aging at 180 °C, at which the highest mechanical characteristics are obtained, a resilience of 25 J/cm^2, a grain size of 140–180 μm, and a maximum depth of the erosion MDEmax around 14–17 μm.

Keywords: aluminum alloy 5083; cavitation erosion; heat treatments

check for updates

Citation: Istrate, D.; Sbârcea, B.-G.; Demian, A.M.; Buzatu, A.D.; Salcianu, L.; Bordeasu, I.; Micu, L.M.; Ghera, C.; Florea, B.; Ghiban, B. Correlation between Mechanical Properties—Structural Characteristics and Cavitation Resistance of Cast Aluminum Alloy Type 5083. *Crystals* **2022**, *12*, 1538. https://doi.org/10.3390/cryst12111538

Academic Editor: Shouxun Ji

Received: 3 October 2022
Accepted: 19 October 2022
Published: 28 October 2022

Publisher's Note: MDPI stays neutral with regard to jurisdictional claims in published maps and institutional affiliations.

Copyright: © 2022 by the authors. Licensee MDPI, Basel, Switzerland. This article is an open access article distributed under the terms and conditions of the Creative Commons Attribution (CC BY) license (https://creativecommons.org/licenses/by/4.0/).

1. Introduction

Aluminum alloys, especially those of the 5083 series, are used in the automotive, aerospace, and transportation industries due to its properties such as low density, high specific strength and excellent corrosion resistance [1–3]. The 5083 series aluminum alloy is an alloy that possesses good hardenability and weldability properties [4]. Alloy 5083, with properties of high corrosion resistance, excellent weldability and good strength, is used in shipbuilding, automotive, and aerospace industries [1–6]. The principal alloying element in aluminum alloy 5083 is magnesium 5 wt% of which induces strong solution hardening effects. It is used in corrosive environments due to its relatively high strength and good corrosion resistance properties [3].

The hardening mechanism of these type 5083 aluminum alloys is due to the formation of the β-phase (Mg_5Al_8). The excess Mg atoms that exist in the matrix are supersaturated

atoms and the remaining Mg atoms are in the form of β-phase [7–12]. An important problem is that following the welding process of 5083 alloy is the grain flow in fusion welding [9]. Liu et al. [10] concluded that considerable softening occurs in alloy 5083 welds due to grain growth. Ma et al. [11] showed in their research that the grain size in the fusion zone increased up to 200 μm, and the base metal grain size was about 50 μm, leading to 15% decrease in tensile strength. Corigliano et al. [12] also showed that 5 mm Al 5083 joints by single-pass GMAW could fail in the thermally affected zone due to stress concentration.

On the other hand, some components, during operation, such as radiators and rotors of vehicle cooling pumps, as well as the propellers of fishing and recreational boats are affected by the abrasive, chemical, and cavitational corrosive action of water. At certain hydrodynamic flow regimes, cavitational corrosion becomes the most dangerous. Operation in such regimes inevitably leads to damage to the structure due to cyclic microjet stresses and shock waves produced by imploding cavitating bubbles. Although the chemical constitution and alloying with other chemical elements enhance the mechanical properties, the lifetime is still limited when operating in high-intensity cavitating flows.

Aluminum alloy type 5083 is mainly used for pressure vessels, products that are used in special temperature conditions, and areas with increased aggressiveness, generally, pieces that require special properties for alloy 5083. The present work aims to define the best combination of heat treatments and erosion–cavitation resistance in these heat-treated states, in order to obtain the best combination of properties obtained from heat treatments of cast products.

2. Materials and Experimental Procedure

Aluminum alloy sample types 5083 were taken in a cast state, without heat treatment, having the chemical composition indicated in Table 1.

Table 1. Chemical composition of experimental alloy specimens 5083.

Sample	Chemical Composition, % Rate								
	Si	**Fe**	**Cu**	**Mn**	**Mg**	**Cr**	**Zn**	**Ti**	**Al**
Experimental	0.41	0.29	0.106	0.52	4.21	0.12	0.16	0.028	Rest
SR EN 373- 3	Max 0.40	Max 0.40	Max 0.10	0.4–1.0	4.0–4.9	0.05–0.25	Max 0.25	Max 0.15	Rest

The following heat treatments were performed on the experimental specimens with dimensions 10 × 10 × 50 (mm): homogenization at 350 °C/with maintenance 100 min followed by air cooling and artificial aging at 180 °C, with three maintenance periods, 1 h, 12 h, and 24 h; homogenization at 450 °C/with maintenance 100 min followed by cooling in air and artificial aging at 140 °C, with three maintenance periods, 1 h, 12 h, and 24 h; homogenization at 450 °C/with maintenance 100 min followed by air cooling and artificial aging at 180 °C, with three maintenance periods, 1 h, 12 h, and 24 h.

The heat treatments were performed in a Nabertherm type furnace, from of the laboratory of Metallic Materials Science, Physical Metallurgy within the University Politehnica of Bucharest. For each type of heat treatment, six tests were performed to determine the mechanical properties: tensile strength, yield strength, elongation, resilience, hardness, and microhardness. The grain size was determined according to ASTM E3, ASTM E 407, and ASTM E 112, using Barker electrolytic reagent, measuring 100. Structural investigations were performed on an OLYMPUS microscope from the Metallic Materials Science and Physical Metallurgy Laboratory from University Politehnica of Bucharest.

The analysis of the samples by X-ray diffraction was performed with the help of the D8 Advance diffractometer, Bruker-Germany, Cu anode tube (λ = 1.540598 Å), and scintillation detector. The diffractograms were recorded with an angular increment of 0.040, at a scanning speed of 0.5 s/step, angular range measuring 2θ = 20–100°.

The experiments concerning cavitational resistance of the experimental samples were made in Cavitation Erosion Research Laboratory of the Polytechnic University of Timișoara, on the vibrating device with standard piezoceramic crystals, using cylindrical vibrating samples, with a diameter of 15.8 mm and 16 mm long [7]. The research conditions on the total duration (165 min), the intermediate periods (one of 5 and 10 min each and 10 of 15 min) on the liquid medium, and the processing and interpretation of the recorded data are in accordance with the laboratory custom [5,7,13–20] and those prescribed in the international standard ASTM G32-2016 [21].

Throughout the research, the functional parameters of the vibrating device, on which depends the intensity of the hydrodynamics of the vibrating cavity, respectively, that of erosion, due to the automated control by a special software, were maintained at standard values [7,21]: double vibration amplitude 50 μm, vibration frequency 20 ± 0.2 kHz, electronic ultrasonic generator power 500 W, distilled water temperature 22 ± 1 °C.

From each type of state (delivered/semi-finished and obtained by heat treatments) five samples were tested, whose experimental values were algebraically mediated in order to build specific cavitation diagrams, which are the basis for analyzing the behavior and strength of exposed surface structures cavity attack.

3. Experimental Results, Interpretations, and Discussions

3.1. Results concerning the Mechanical Behavior of the Experimental Samples

The experimental results regarding the determination of the mechanical characteristics are presented in Table 2. The analysis of the evolution of the values of the mechanical characteristics comparatively for each specimen is presented successively in Figures 1–5. From the graph of Figure 1, it can be noticed that the values of tensile strength increase significantly by applying heat treatment. After homogenization and aging at 180 °C, different durations of maintenance, the highest values are obtained, respectively, 318 MPa for maintenance at 1 h (44% higher than the value of the control sample), followed by 346.20 MPa, at 12 h maintenance, (increase by 57%) and the highest value after 24 h, respectively, 436 MPa (increase by approximately 100%).

The evolution of yield strength is given in Figure 2. As one may remark, the increasing this property is only after 350 °C + 180 °C, at any other heat treatment this increase is with no importance. Elongation property decreases by applying different heat treatments, as is given in Figure 3. Considering only elongation, the recommended heat treatment is at 450 °C + 140 °C/1, 12, 24 h. In Figure 4 one may remark that the hardness values may increase with the time of maintaining at the same aging temperature, the highest values being for 450 °C + 140 °C/ 24 h. As is given in Figure 5, one may remark a slight modification regarding hardness values after applying different heat treatments. Generally, the hardness values are between 72 and 82 daN. The most important property for cast products made of 5083 aluminum alloy is resilience, whose evolution is given in Figure 5. As one may remark, considering as admitted value is 25 J/cm^2, only homogenization at 350 °C + 180 °C is proper to maintain high values of resilience. At any other heat treatment, the increasing of the time of maintenance leads to drastically diminishing the resilience, reaching very low values, 18–22 J/cm^2.

Table 2. Mechanical behavior and grain size of the experimental samples type 5083 in different structural states.

State		Mechanical Characteristics											
		Tensile Strength		Yield Strength		Elongation		Hardness		μHV		Resilience	
		[MPa]	Std Dev	[MPa]	Std Dev	[%]	Std Dev	[daN]	Std Dev	μHV	Std Dev	[J]	Std Dev
H	Gauge sample	220.63	±0.9959	118.84	±1.07078	28.40	±0.34139	79.80	±0.50992	76.97	±0.81134	32.12	±1.05334
HAP	350 °C/100 min/air + 180 °C/1 h	318.58	±1.00659	151.21	±0.7681	17.11	±0.61917	76.80	±0.8697	76.89	±1.34867	31.00	±0.7858
HAL	350 °C/100 min/air + 180 °C/12 h	346.20	±1.19915	195.70	±1.92787	14.75	±0.58161	79.00	±0.8696	79.14	±0.83814	25.80	±0.7305
HAI	350 °C/100 min/air + 180 °C/24 h	436.30	±1.29539	356.68	±0.90159	12.73	±0.66545	79.00	±0.66545	80.01	±0.58868	25.20	±0.38525
HNOP	450 °C/100 min/air + 140 °C/1 h	294.82	±0.64895	139.57	±1.13429	23.44	±0.76294	72.80	±0.9508	74.65	±0.79193	32.60	±0.8542
HNOL	450 °C/100 min/air + 140 °C/12 h	307.63	±1.25037	141.66	±0.82781	21.17	±0.78856	76.80	±1.01068	75.30	±1.00258	22.10	±0.69215
HNOI	450 °C/100 min/air + 140° C/24 h	311.21	±0.80242	144.55	±1.86119	19.18	±0.96929	76.80	±1.03349	80.67	±0.72652	18.00	±0.73799
HNP	450 °C/100 min/air + 180 °C/1 h	250.03	±0.78143	146.50	±1.16986	12.68	±0.6629	71.80	±0.53337	78.12	±0.58145	31.70	±0.62006
HNL	450 °C/100 min/air + 180 °C/12 h	315.16	±1.02569	149.91	±0.83089	13.18	±0.54174	77.90	±0.62742	78.38	±0.83996	28.40	±0.89793
HNI	450 °C/100 min/air + 180 °C/24 h	318.34	±1.60049	158.62	±1.08443	14.44	±0.54551	80.70	±0.60322	79.68	±1.09967	16.40	±0.70432

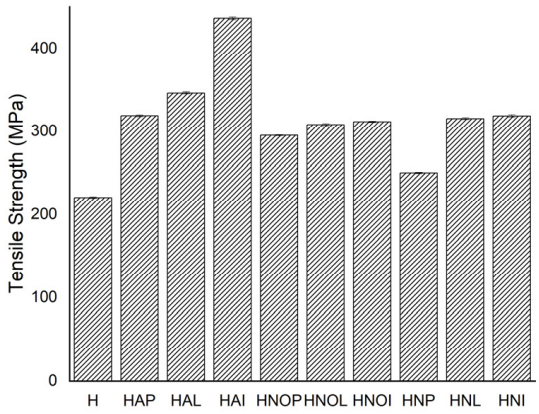

Figure 1. Evolution of tensile strength values of the experimental 5083 alloy samples, in different structural state.

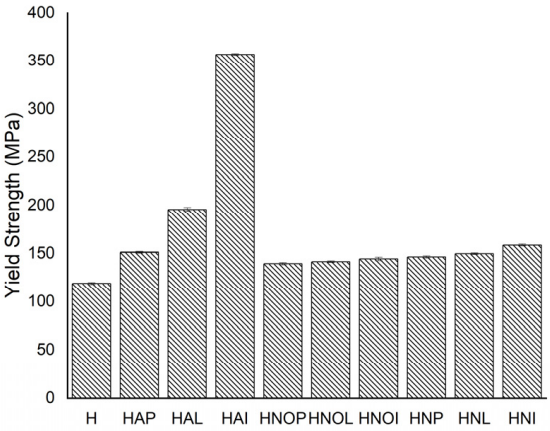

Figure 2. Evolution of yield strength values of the experimental 5083 alloy samples, in different structural states.

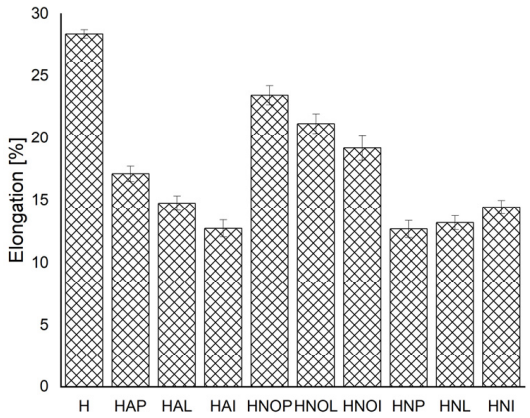

Figure 3. Evolution of elongation values of the experimental 5083 alloy samples, in different structural states.

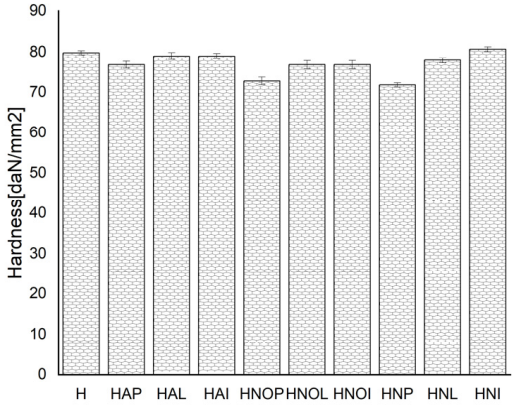

Figure 4. Evolution of hardness values of the experimental 5083 alloy samples, in different structural states.

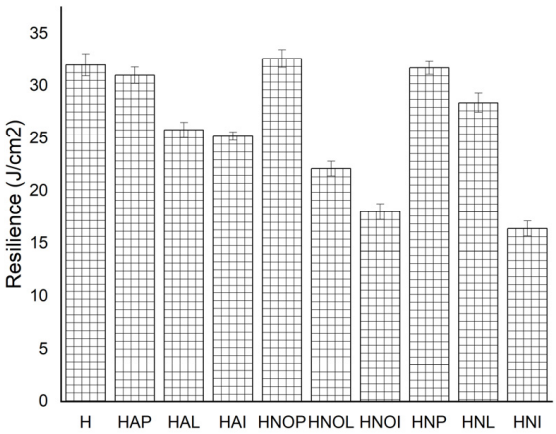

Figure 5. Evolution of resilience strength values of the experimental 5083 alloy samples, in different structural states.

3.2. Results concerning Structural Characterization of the Experimental Samples

Results concerning the structural analysis of the experimental samples concerning metallographic aspects after applications of different heat treatments of the cast aluminum 5083 samples are given in Figure 6. One may remark that at the gauge sample there is a dendritic aspect of the sample (Figure 6a), with small amounts of particles, precipitated in a dendritic manner. By applying quenching and aging, it takes place the homogenization of the matrix, the particles being still in dendritic separation (Figure 6b–j). Additionally, one may remark that in gauge samples there are the biggest gains, in a nonhomogeneous solution, and after applying quenching at 450 °C there are obtained structures with smaller grain sizes than after quenching at −350 °C.

The experimental results regarding the determination of the grain size after statistical analysis of the experimental specimens are shown in Table 3. It is noted that in the control sample the average grain size is at the highest level, around 255 μm. By applying heat treatments, the diminishing of the granulation takes place. At quenching and aging at 350 °C + 180 °C the average grain size is in general higher than at 450 °C + 180 °C or 450 °C + 140 °C. The graph of the grain size varies depending on the heat treatment applied to the experimental samples as shown in Figure 7.

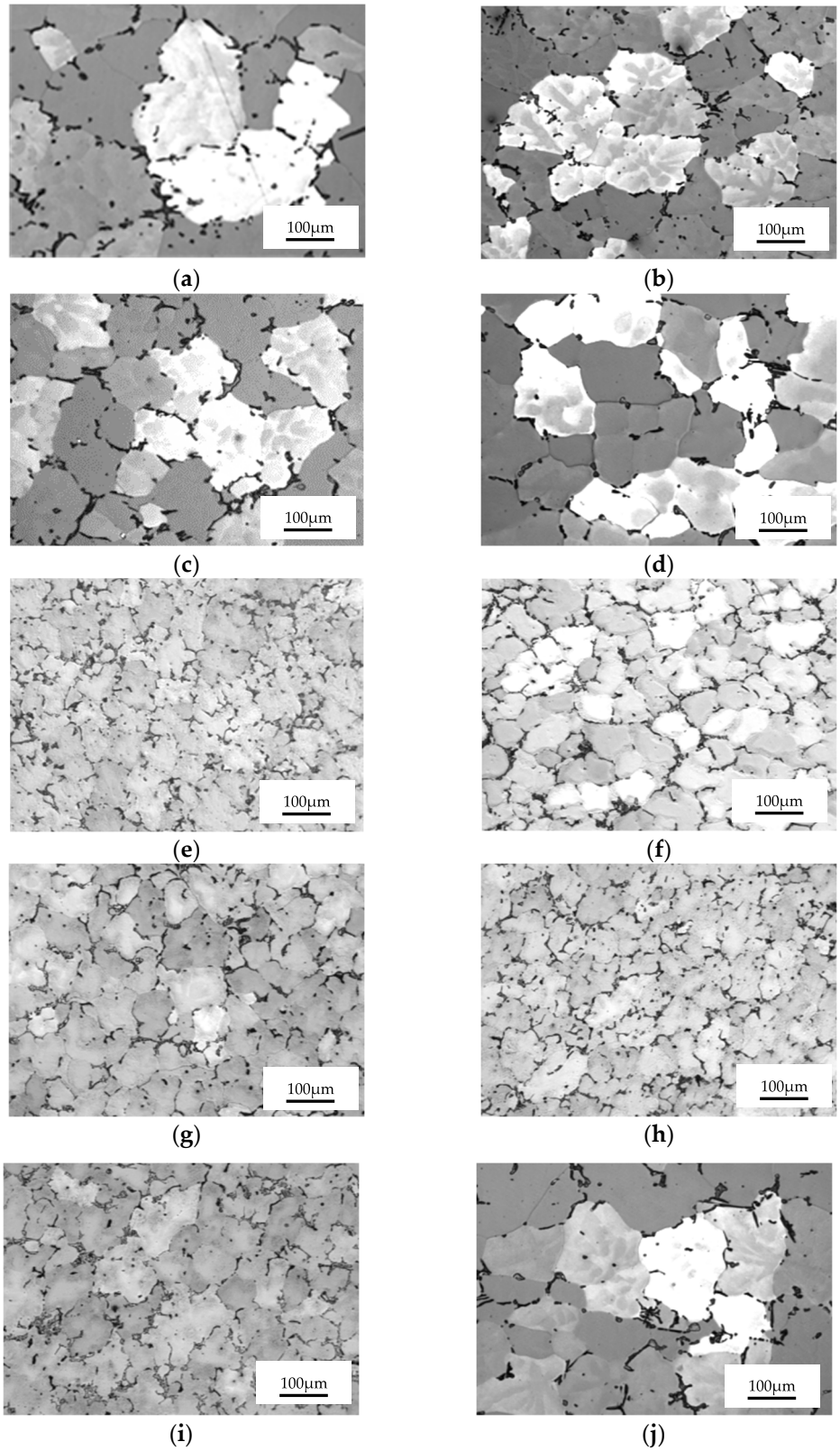

Figure 6. Structural analysis of cast experimental samples from aluminum 5083 alloy: (**a**) Gauge sample (H), (**b**–**d**) cast + quenched at 350 °C/100 min/air + artificial ageing at 180 °C; (**e**–**g**) cast + quenched at 450 °C/100 min/air + artificial ageing at 140 °C; (**h**–**j**) cast + quenched at 450 °C/100 min/air + artificial ageing at 140 °C (**b**,**e**,**h**) 1 h maintaining, (**c**,**f**,**i**) 12 h maintaining, (**d**,**g**,**j**) 24 h maintaining.

Table 3. Grain size analysis of the experimental alloy type 5083.

Code	State	Parameters of the Statistical Analysis				
		Grain Size Minimum [µm]	Grain Size Maximum [µm]	Grain Size Medium [µm]	Standard Deviation [µm]	95% CI [µm]
H	Gauge sample	120.10	653.51	255.95	94.17	20.17
HAP	350 °C/100 min/air + 180 °C/1 h	10.03	317.86	185.58	77.08	27.33
HAL	350 °C/100 min/air + 180 °C/12 h	41.89	302.18	164.05	52.34	16.15
HAI	350 °C/100 min/air + 180 °C/24 h	36.89	272.76	149.69	51.21	14.78
HNOP	450 °C/100 min/air + 140 °C/1 h	20.10	425.23	212.29	83.05	12.17
HNOL	450 °C/100 min/air + 140 °C/12 h	20.10	475.53	197.06	96.01	14.51
HNOI	450 °C/100 min/air + 140 °C/24 h	20.10	426.54	190.38	97.38	13.94
HNP	450 °C/100 min/air + 180 °C/1 h	21.84	564.23	245.23	108.83	19.01
HNL	450 °C/100 min/air + 180 °C/12 h	49.02	418.34	225.31	43.57	18.52
HNI	450 °C/100 min/air + 180 °C/24 h	103.10	371.86	215.21	36.28	16.83

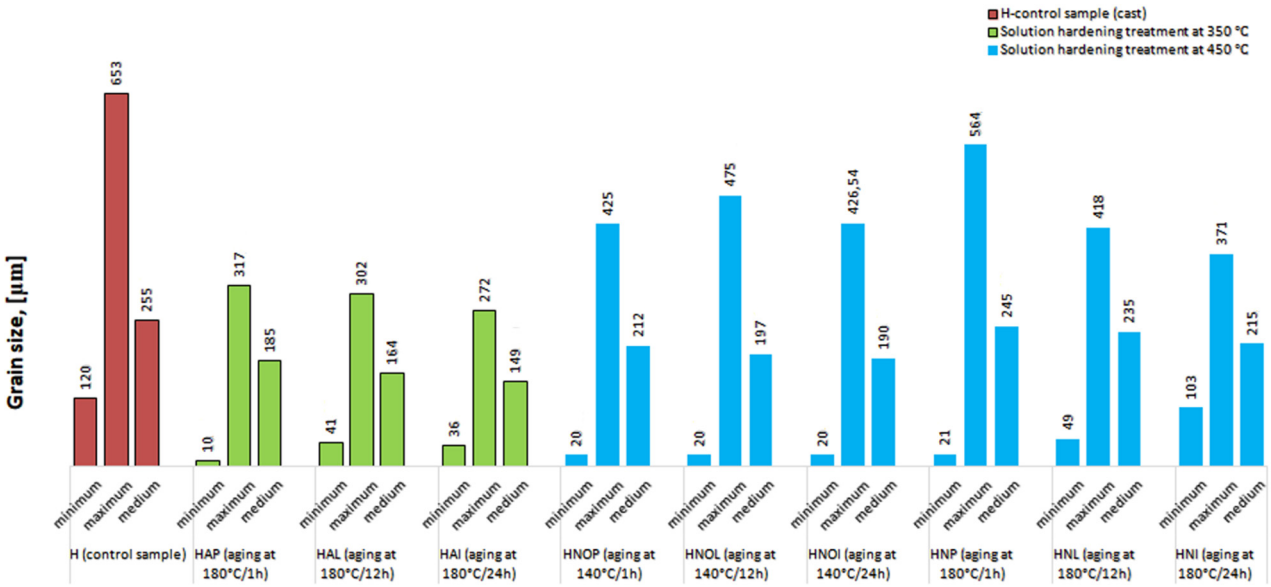

Figure 7. Evolution of grain size values of the experimental 5083 alloy samples, in different structural state.

3.3. X-rays Diffraction Analysis

Qualitative X-ray diffraction phase analysis revealed the polycrystalline nature of the analyzed samples. The appearance of the diffractograms for the specimens subjected to the various heat treatments is shown in Figure 8. The crystallographic phases were identified according to the ICDD Release 2015 database, PDF 01-074-5237. The parameters of the elementary cell, respectively, and the size of the crystallite were calculated using the Rietveld method and correspond to Al0.95Mg0.05, represented in Table 4. The proportion of Mg_5Al_8 secondary phases is very small, better identification of which can be achieved by analysis with a scanning electron microscope. A careful analysis of the values of the elements of the elementary cell revealed the fact that applying heat treatments to hardening and aging can lead to the modification of this parameter. The combination 450 °C + 140 °C leaves the element cell parameter unchanged, respectively, 4.073 [Å], compared to the

control sample. In contrast to the other heat treatments there is an increase in the network parameter, either in the range 4.072–4.075 [Å] when applying the heat treatments 350 °C + 180 °C, or an increase in the network parameter in the range 4.074–4.076 [Å] when applying heat treatments at 450 °C + 180 °C.

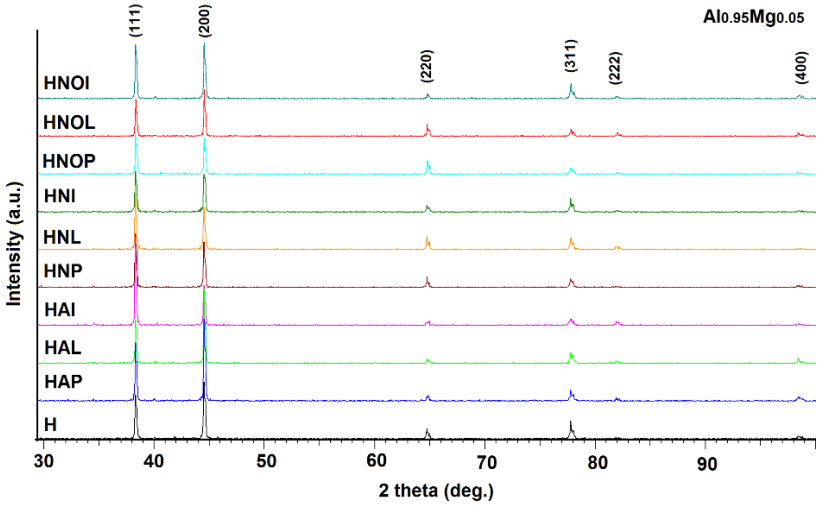

Figure 8. Appearance of X-ray diffractograms of 5083 aluminum alloy samples after heat treatment at different temperatures and maintenance times.

Table 4. Elemental cell parameters and crystallite size of the analyzed samples.

Test Code	Crystallographic Phase	Elementary Cell Parameters, a [Å]	Crystalline Size
			D (nm)
H	Al0.95Mg0.05	4.073	163.2
HAP		4.075	150.8
HAL		4.074	140.3
HAI		4.072	136.5
HNOP		4.073	162.2
HNOL		4.073	145.6
HNOI		4.073	145.6
HNP		4.076	158.4
HNL		4.075	151.2
HNI		4.074	123.9

3.4. Determination of the Behavior of Experimental Specimens in Cavitational Corrosion

The results regarding the behavior of cavitational erosion are expressed either in the form of graphs such as average erosion depth (MDE)/average penetration rate of cavitation erosion depending on the duration of the corrosive attack (Figure 9), indicated in international standards ASTM G 32-2016 [21] or by analysis under an optical/stereomicroscopic (Figures 10–13) or the scanning electron microscope, Figure 14.

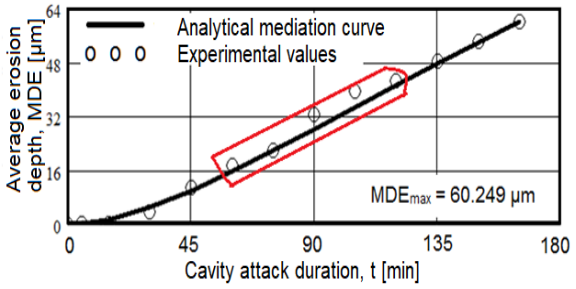

(**a**)

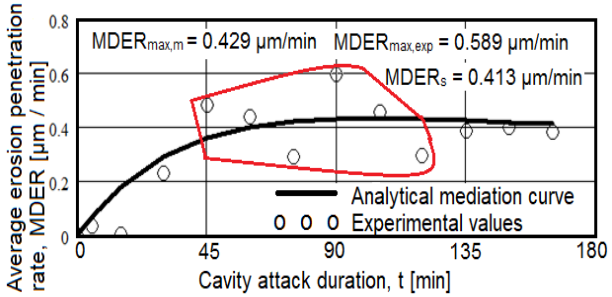

(**b**)

(A = 0.038, B = 0.02)

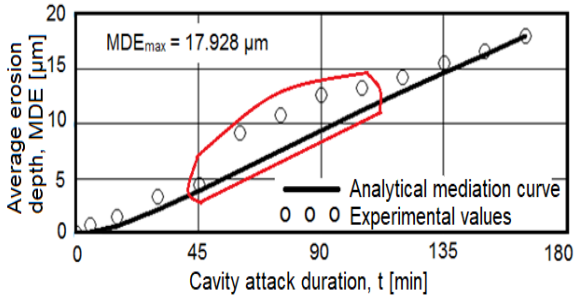

(**c**)

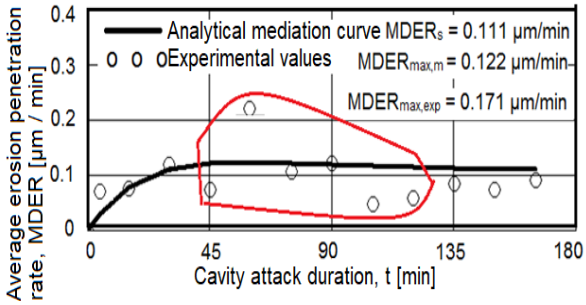

(**d**)

(A = 0.109, B = 0.035)

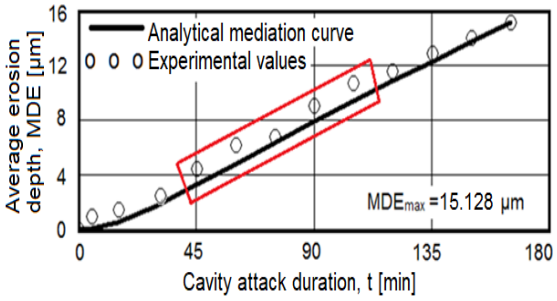

(**e**)

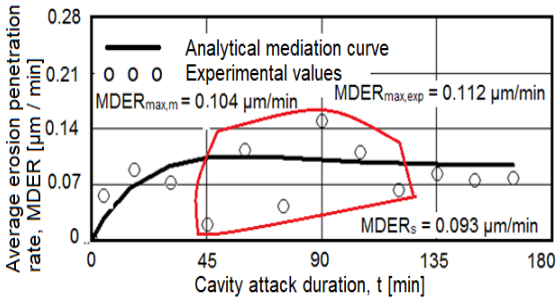

(**f**)

(A = 0.092, B = 0.034)

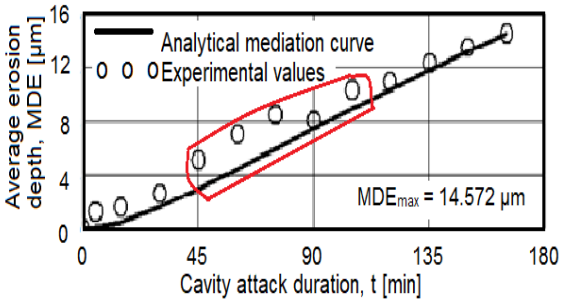

(**g**)

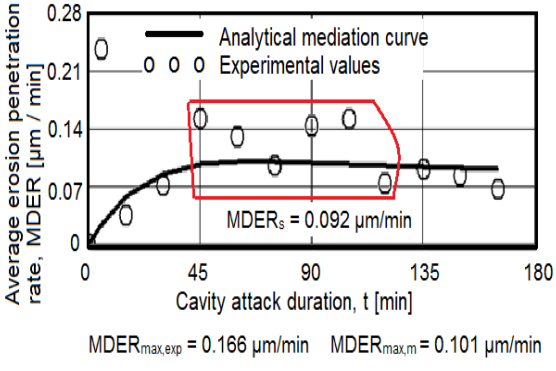

(**h**)

(A = 0.089, B = 0.03)

Figure 9. *Cont.*

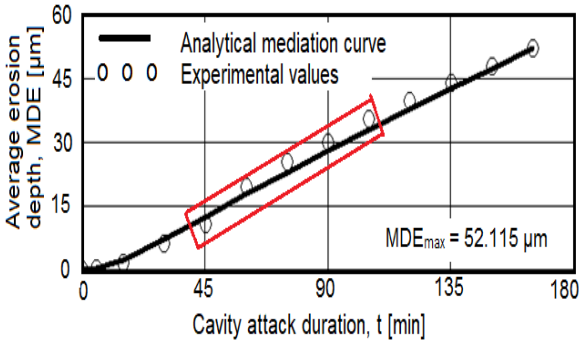

(**i**)

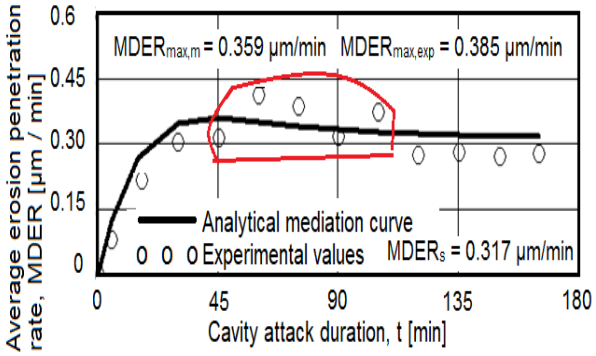

(**j**)

(A = 0.233, B = 0.034)

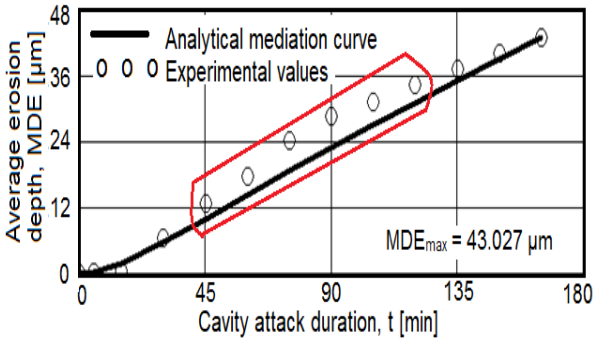

(**k**)

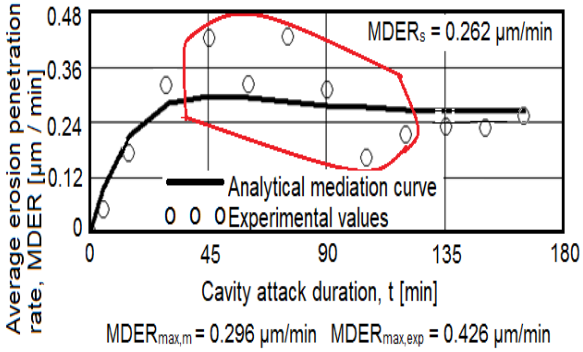

(**l**)

(A = 0.261, B = 0.043)

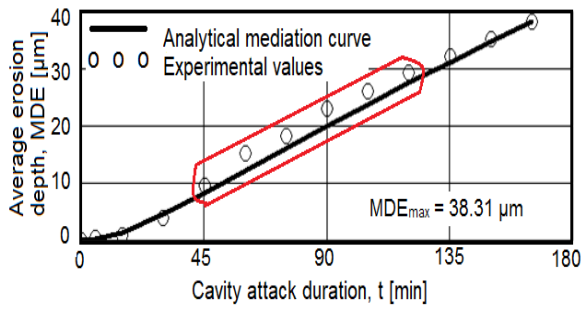

(**m**)

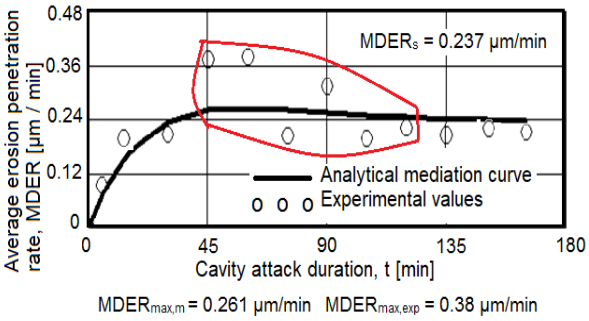

(**n**)

(A = 0.316, B = 0.046)

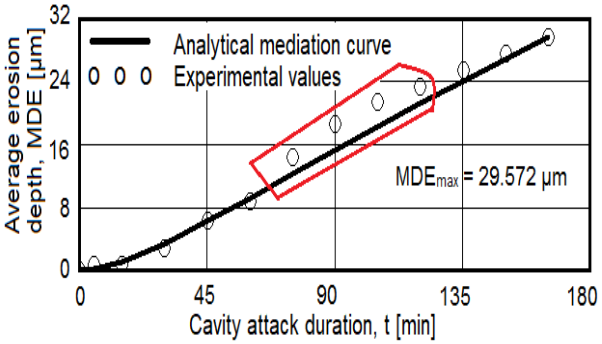

(**o**)

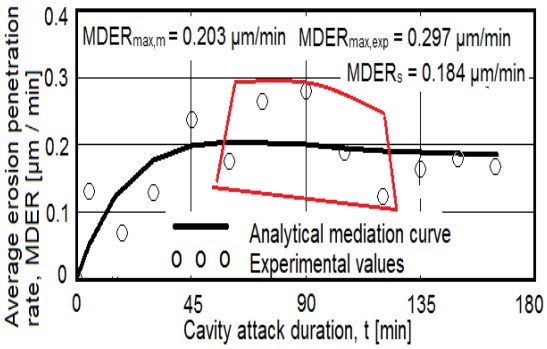

(**p**)

(A = 0.18, B = 0.32)

Figure 9. *Cont.*

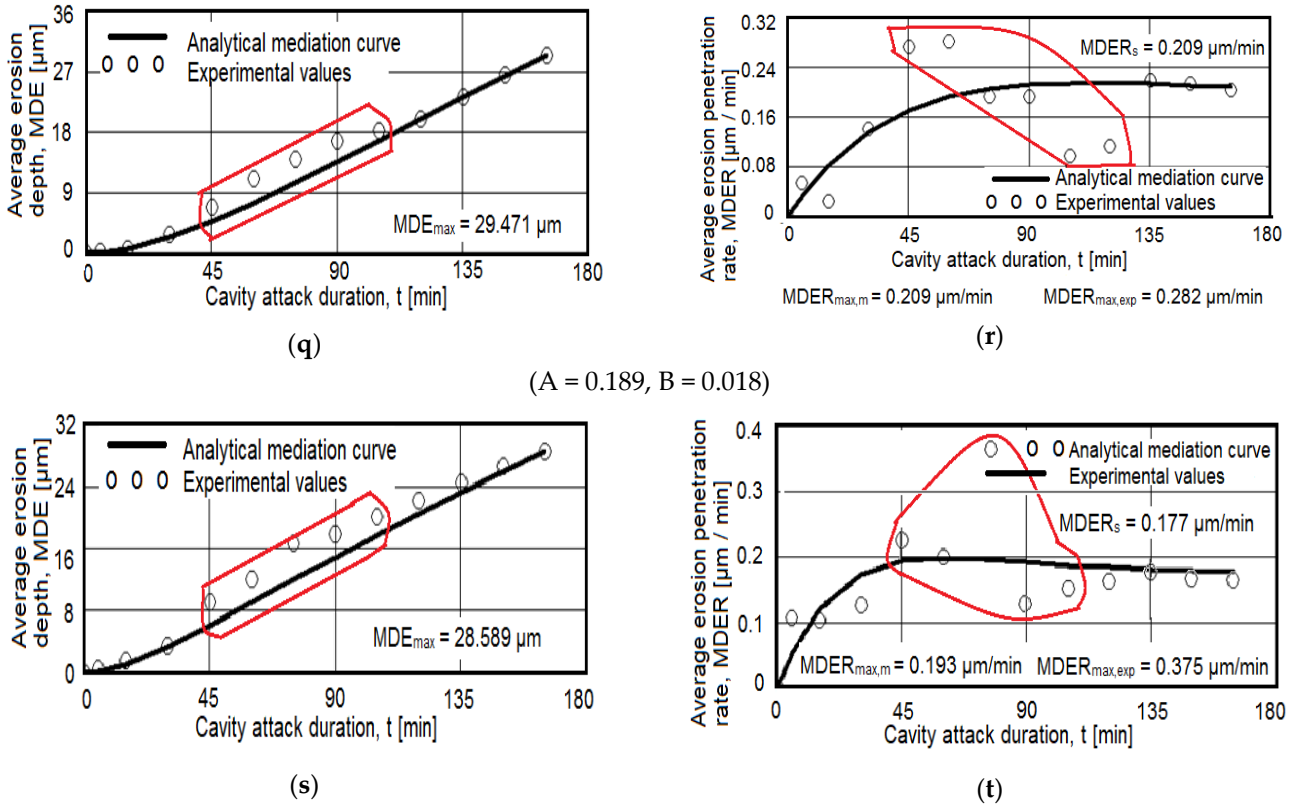

Figure 9. Average erosion depth (**a**,**c**,**e**–**i**,**k**,**m**,**o**,**q**,**s**) and average erosion rate (**b**,**d**,**f**,**h**,**i**,**l**,**n**,**s**,**t**) versus cavitation exposure time of the experimental samples of aluminum type 5083: (**a**,**b**) gauge sample, (**c**–**h**) after 350 °C/100 min/air + 180 °C, (**i**–**n**) after 450 °C/100 min/air + 140 °C, (**o**–**t**) after 450 °C/100 min/air + 180 °C, (**c**,**d**,**i**,**j**,**o**,**p**) 1 h maintainig, (**e**,**f**,**k**,**l**,**q**,**r**) 12 h maintaining (**g**,**h**,**m**,**n**,**s**,**t**) 24 h maintaining 200×, (**c**) 500×, (**d**) 2000×.

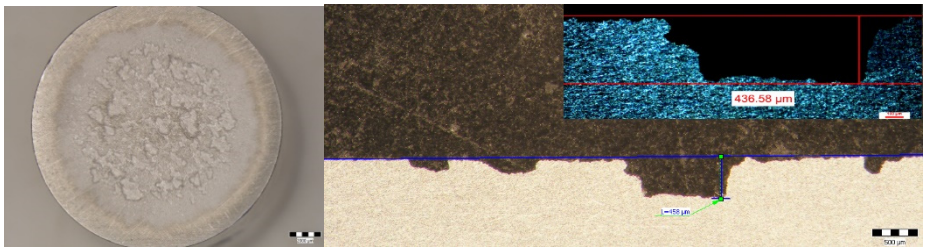

Figure 10. Appearance of macrostructural surfaces (left front section, parallel to the eroded surface, right in cross section, background optical microscope image, detailed stereomicroscope image) subjected to cavitation erosion of alloy 5083, in cast state.

The diagrams containing the experimental values of the erosion test, with a total duration of 165 min, and the mediation curves MDE (t) and MDER (t) built with the statistically established relationships within the Cavity Erosion Research Laboratory [22] are presented in Figure 9. The areas marked by dark red curves include the experimental values that express the yield of surface material to the impact with the cavitation microjet which, in a significant duration of the cavitation (depending on the duration of maintenance to the artificial aging treatment) degrades by expanding the caverns in area and depth. At the same time, it is noted that after about 120 min of cavitation, until the end of the experiment (165 min), the mass loss, respectively, average depth of erosion, and their erosion rates have non-significant evolution. From the experiences of the laboratory [16,17,19,20,23] and

other authors [7,24,25], we consider that this behavior, towards the end of the experiment, is caused by the air entering the caverns during the surface vibration, which dampens the impact pressure/shock between the surface exposed with the shock wave and the micro-jets produced by the implosion of the cavitation bubbles.

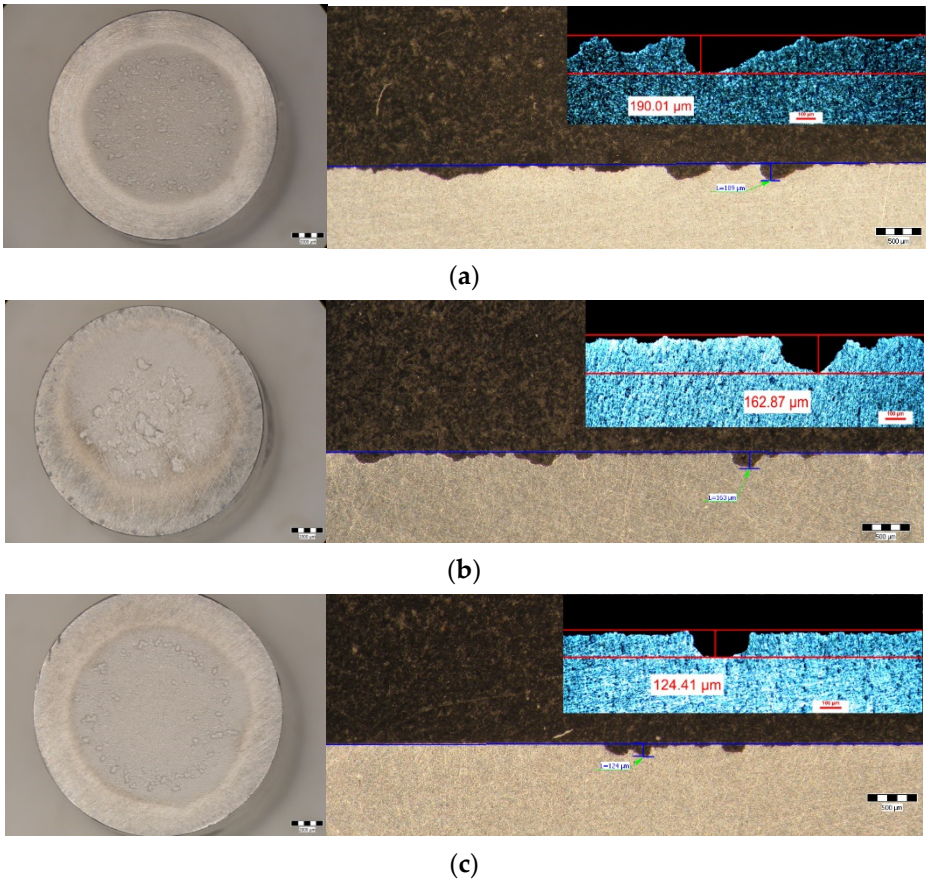

Figure 11. Appearance of macrostructural surfaces (left front section, parallel to the eroded surface, right in cross section, background image under an optical microscope, detail image under a stereomicroscope) subjected to cavitation erosion from alloy 5083, poured followed by hardening solution 350 °C/maintenance 100 min/cooling air quietly and subjected to artificial aging at 180 °C and different maintenance times: (**a**) 1 h; (**b**) 12 h; (**c**) 24 h.

A careful analysis of these graphs, the comparative results of which are illustrated in Table 5, shows that the 5083 alloy specimens have similar behavior, with the same erosion mechanisms, specific to the class of aluminum alloys, much different from the erosion mechanisms found in other classes of metallic materials hardened by solid-state transformations [18,26]. The following aspects can be highlighted:

- The most significant losses, with the development of pinches and caverns in the area of the exposed surface, are registered in the interval 45–120 min (large differences between the experimental, successive values of the measured parameters MDE and MDER, as well as large deviations from the MDE mediation curves (t), respectively, MDER (t)) for all experimental specimens;
- In the first 30 min there is an erosive mechanism by which the roughness tips, and abrasive dust are removed and elasto-plastic deformations and crack networks occur [16,20,23];
- The shape of the approximation/mediation curve of the experimental values has different values between maximum value ($MDER_{max}$), and that value which tends to stabilization of the process (final value $MDER_s$) (as can be seen from Table 6, registering

differences of about 0–12%). This difference, manifested in all situations, is specific to surfaces with average mechanical properties in a value (with values of hardness of about 80 HB and resilience of about 25 J), which gives this condition a behavior specific to materials with a low resistance to cavitation [20,21,23,27–29];

- There are insignificant differences in all heat treatment situations between the experimental values of the erosion rates after 120 min and until the end of the test, which leads to an approximately linear increase in the MDE curve (t) over this time interval and slightly asymptotic stabilization of the MDER curve (t), differences of the structural plastic characteristics which may decrease the resistance to cyclic stresses of cavitation micrometers;
- There is a big difference (which, as indicated in Table 6, is in the range of 8–94%) between the maximum value obtained by the experiment (MDER $_{max.exp}$) and that defined by the mediation curve (MDER $_{max,m}$), even if it is recorded at the same duration of the cavitation (90 min). The smallest difference is recorded in the heat-treated sample at 450 °C/100 min/air + 140 °C/12 h/air of about 8%, and the largest difference is recorded in the heat-treated sample at 450 °C/100 min/air + 180 °C/12 h/air of about 94%. In the other heat treatment states, this difference is in the range of 40–65%. This aspect is further proof of the complexity of the mechanism by which the structure responds to the cavitation load and by which the effect of the duration of maintenance at the temperature of the heat treatment on the structure and mechanical properties, as value and mode of distribution in the sample volume.

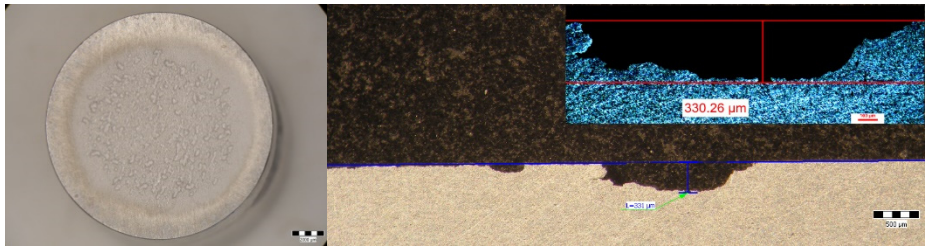

(**a**)

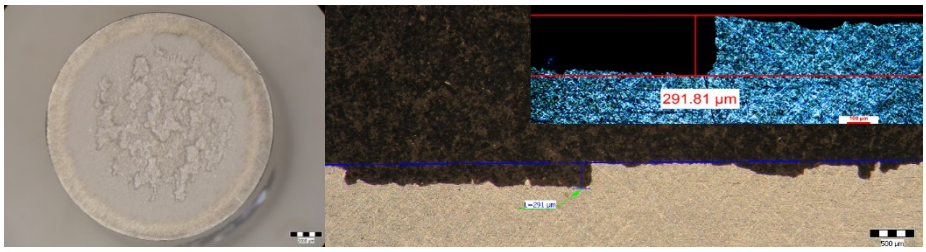

(**b**)

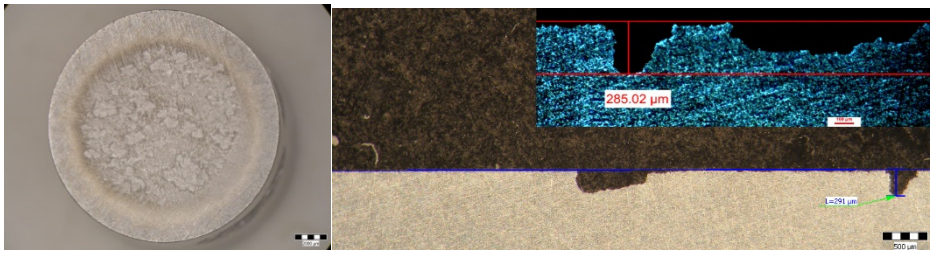

(**c**)

Figure 12. Appearance of macrostructural surfaces (left front section, parallel to the eroded surface, right in cross section, background image under an optical microscope, detail image under a stereomicroscope) subjected to cavitation erosion from alloy 5083, poured followed by hardening solution 450 °C/maintenance 100 min/cooling air quietly and subjected to artificial aging at 180 °C and different maintenance times: (**a**) 1 h; (**b**) 12 h; (**c**) 24 h.

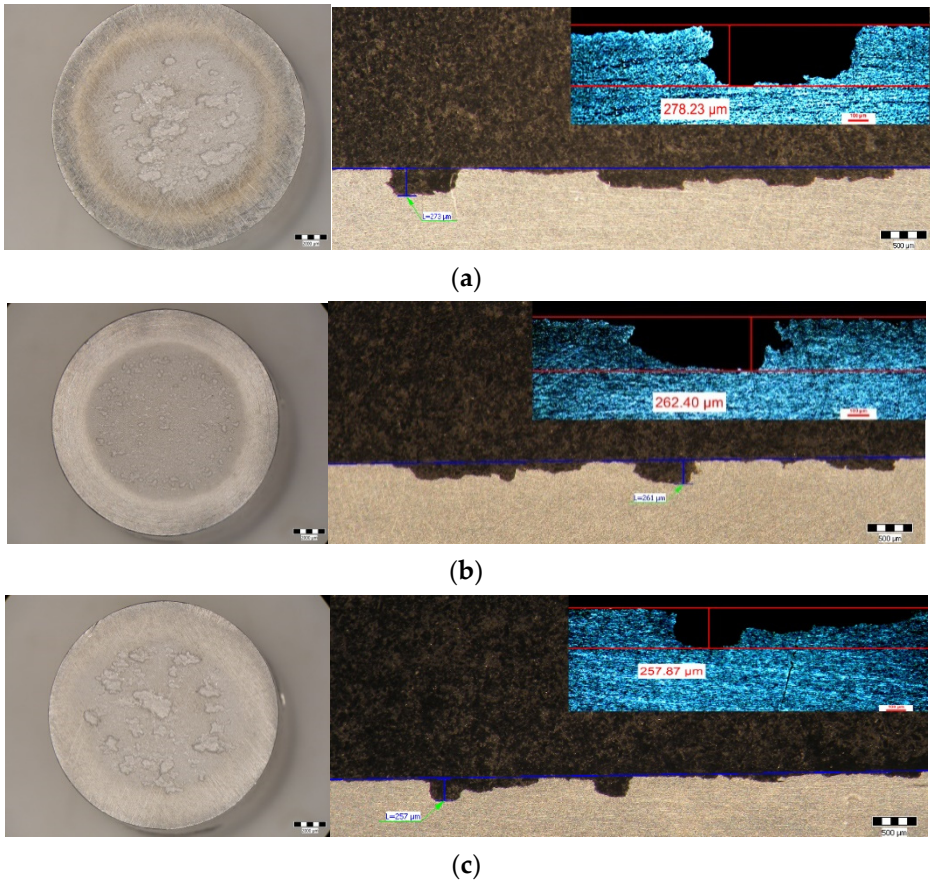

Figure 13. Appearance of macrostructural surfaces (left front section, parallel to the eroded surface, right in cross section, background optical microscope image, detailed stereomicroscope image) subjected to 5083 alloy cavitation erosion, cast followed by solution hardening 450 °C/maintenance 100 min/cooling quiet air and subjected to artificial aging at 140 °C and different maintenance times: (**a**) 1 h; (**b**) 12 h; (**c**) 24 h.

Table 5. Parameters of erosion–cavitation process of the experimental 5083 aluminum samples.

Sample	$MDER_{maxm}$	$MDER_{maxexp}$	$MDER_s$	Δ			
				$\lvert MDER_{maxm} - MDER_{maxexp} \rvert$		$\lvert MDER_{maxm} - MDER_{maxs} \rvert$	
				µm/min	%	µm/min	%
H	0.429	0.589	0.413	0.16	37	0.016	5.7
HAP	0.122	0.171	0.111	0.049	40	0.011	9
HAL	0.104	0.112	0.112	0.008	8	0.008	8
HAI	0.101	0.166	0.092	0.065	65	0.009	9
HNOP	0.101	0.166	0.092	0.065	65	0.009	9
HNOL	0.359	0.385	0.317	0.03	8	0.042	12
HNOI	0.296	0.426	0.262	0.13	44	0.034	12
HNP	0.261	0.380	0.237	0.109	46	0.014	9
HNL	0.109	0.282	0.209	0.073	35	0	0
HNI	0.193	0.375	0.177	0.182	95	0.0.16	8

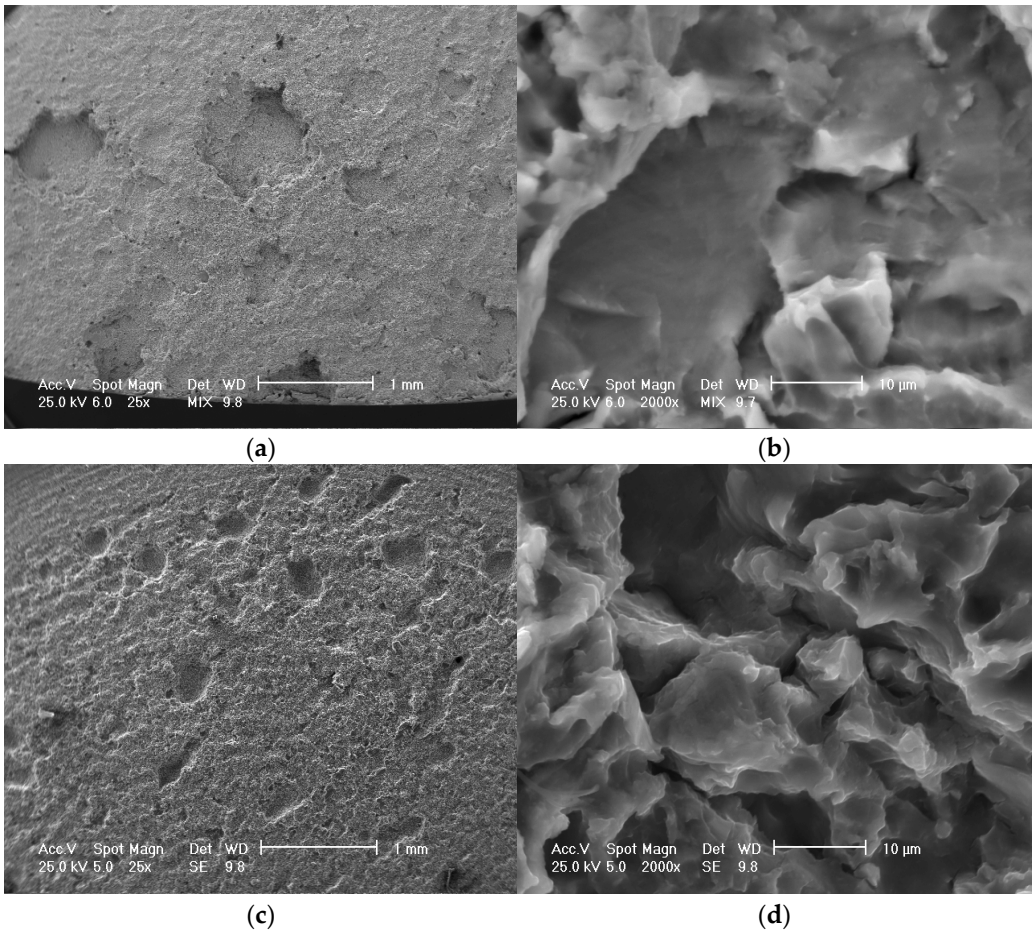

Figure 14. Scanning electron analysis (SEM) of the eroded surfaces of alloy 5083, in cast state (**a**,**b** control sample), and after quenching at 450 °C maintaining 100 min/air cooling and ageing at 180 °C/12 h at different magnification of the microscope (**c**,**d**): (**a**,**c**) macroscopic aspect, (**b**,**d**) microscopic aspect (detail of an image).

The morphological analysis of the eroded structure is given comparatively after the metallographic analysis in Figure 10 (for the control sample) and Figures 11–13 (for the heat-treated samples). The cavitational erosion of the surface starts as early as 15–30 min, but substantial, large losses, with the creation of deep caverns in the form of crevices, take place in the interval of 60–120 min. From the 135th minute, the caverns deepen, and the losses are close, causing approximately constant erosion rates. The causes are the ones mentioned (the amount of air entering and the degree of hardening of the layer impacted by the cavitation microgrids). The macrostructural aspects highlighted under the stereomicroscope show the extension of the cavitational attack in the frontal section. The control sample (Figure 10) has the largest surface affected by the cavitational attack, while the heat-treated specimens at 350 °C/100 min/air + 180 °C show the smallest areas affected by the cavitational attack. The detailed cross-sectional analysis of the surfaces required for cavitation (the images on the right of Figures 10–13) allowed both the visualization of the profile and the determination of the maximum penetration depth of the cavitation attack. There is a huge difference between the value of the maximum measured depth of the cavern caught in the section plane (in the range 125–451 µm, Figures 10–13) and the maximum cumulative average calculated after 165 min (in the range 14–60 µm, Figure 9), a difference of about 6–11 times. It is reconfirmed that for the evaluation of the behavior and strength of a structure at the request of the cavity it is recommended to use the average value on the surface MDE_{max} and not the maximum of a cave, in an arbitrary area. However, the very high value of the pit trapped in the section plan raises a big question mark as to

the degree of fineness and the constitution of the structure of an aluminum alloy with or without preliminary heat treatment. This behavior can give clues about the mechanism of the cavitational phenomenon between different structural classes of metallic materials. Where the surface hardening mechanism takes place in volume, following a transformation into a solid state with martensite formation, then the differences are minimal [20,30]. Where the surface hardening mechanism occurs only by hardening the solid solution (such as aluminum alloys), then the differences are particularly high due to the formation of deep local caverns around the hardening particles in a mass of solid solution unaffected by the cavitational attack.

The analysis of cavitation eroded surfaces under a scanning electron microscope completes the information on the morphology of the surfaces, as well as on the mechanism of propagation of cavitational cracks in this class of metallic materials. Thus, as noted in Figure 14a,b, in the case of a sample not subjected to heat treatment, in a cast state, on a macroscopic scale the surface appears eroded almost uniformly with numerous cavities spread over large areas with polygonal shapes (Figure 14a). On microscopic analysis (Figure 14b) the surface of the bottom of the cavity is cleavage-like, brittle, faceted, and delimited by numerous secondary cracks.

In the heat-treated samples, the appearance of the cavitationally eroded surfaces is approximately similar, especially in the frequency of the cavities, as well as the microscopic appearance. Thus, for example on a heat-treated surface at 450 °C/100 min/air + 180 °C/12 h/air (Figure 14c) on a macroscopic scale, the surface has a high frequency of cavities, with rounded edges, of relatively small dimensions (0.1–0.5 mm). On microscopic analysis (Figure 14d) the surface has a fragile appearance, with cleavage, faceted, with numerous intergranular secondary cracks. SEM analysis confirms the brittle behavior of the 5083 aluminum alloy after cavitation erosion, the cavities produced being generated by the secondary particles of the alloy, around which the structural integrity is destroyed. There is no volumetric hardening of the material by the formation of a hard phase with high mechanical properties (such as martensite), but only a hardening of the solid solution by precipitation of secondary phases (as in the case of aluminum alloy 5083 (with hardening phase Mg_5Al_8), in as a result of the jet's interaction with the surface, the particles dislocate, leaving an eroded surface with numerous intergranular secondary cracks.

Table 6. Maximum depth of penetration of cavitation attack of 5083 aluminum alloy specimens in different heat treatment conditions.

Sample	Maximum Penetration Depth of the Cavitation Attack		
	$MDER_{max}$ (μm)	$\delta_{measured}$ (μm)	$\frac{\delta}{MDER_{max}}$
H	60.249	436.58	7
HAP	17.928	190.01	11
HAL	15.128	162.87	11
HAI	14.572	124.41	8
HNOP	52.115	330.26	6
HNOL	43.027	291.81	7
HNOI	38.31	285.02	7
HNP	29.572	278.23	9
HNL	29.471	262.4	9
HNI	28.589	257.87	9

The comparative analysis of the mechanical behavior and the cavitation erosion behavior of the aluminum alloy samples type 5083, as is given in Table 6, allows the formulation of the following interesting observations:

- By applying heat treatments to 5073 alloy castings, either hardening of the solution at 350 °C/100 min + artificial aging at 180 °C (1 h, 12 h, 24 h), or hardening of the solution at 450 °C/100 min + artificial aging at 140 °C (1 h, 12 h, 24 h) or solution hardening 450 °C/100 min + artificial aging at 180 °C (1 h, 12 h, 24 h) can increase the resistance to cavitational corrosion, in the sense of decreasing the depths of penetration to erosion;
- Within the same combination of heat treatments, increasing the duration of maintenance to artificial aging causes a decrease in the maximum depths of penetration of the cavities. Thus, after hardening of the solution at 350 °C/100 min + 180 °C (Figure 9c–h) the maximum penetration depth of the MDEmax cavity decreases from 17.928 μm (at maintenance 1 h), at 15.128 μm (at maintenance 12 h), reaching 14.572 μm (at maintenance 24 h). After hardening the solution at 450 °C/100 min + 140 °C (Figure 9i–n) the maximum penetration depth of the MDEmax cavity decreases from 52.115 μm (at maintenance 1 h), at 43.017 μm (12 h maintenance), reaching 38.31 μm (24 h maintenance). After hardening the solution at 450 °C/100 min + 180 °C (Figure 9o–t) the maximum penetration depth of the MDEmax cavity decreases from 29.572 μm (at maintenance 1 h), at 29.471 μm (12 h maintenance), reaching 28.589 μm (24 h maintenance);
- After applying a solution hardening at 350 °C/100 min + artificial aging at 180 °C, the lowest penetration depths of the cavity are obtained both compared to the control sample, with 60 μm, and compared to the samples subjected to hardening solution at 450 °C/100 min + artificial aging (either at 140 °C where the maximum depth of penetration is 38–52 μm, or at 180 °C, where the maximum penetration depth is about 29 μm);
- The correlation between the highest mechanical characteristics obtained after applying a solution hardening at 350 °C/100 min + artificial aging at 180 °C (1 h, 12 h, 24 h) and the behavior at cavitational erosion, which is the more favorable to these heat treatments applied to 5083 aluminum alloy castings.

4. Conclusions

The following conclusions can be drawn from the experiments carried out in this paper:

- By applying homogenization heat treatments, the mechanical and structural characteristics of 5083 alloy cast products can be modified. So, the values of breaking strength and yield strength change similarly. The elongation values are intermediate for homogenization at 350 °C, compared to homogenization at 450 °C, regardless of the duration of aging. Hardness values decrease slightly after applying homogenization at 350 °C + 180 °C (only 1–4%), compared to homogenization at 450 °C + 140 °C, where the hardness decreases reach up to 10% compared to gauge sample.
- The lowest values of the average grain size are recorded at homogenizations at 350 °C + 180 °C, average sizes for homogenization at 450 °C + 140 °C and the highest grain sizes for 450 °C + 180 °C.
- By applying heat treatments to 5073 alloy castings, we can increase the resistance to cavitational corrosion, in the sense of decreasing the depths of penetration and erosion penetration rate. Within the same combination of heat treatments, increasing the duration of maintenance to artificial aging causes a decrease in the maximum depths of penetration of the cavities. Thus, after hardening of the solution at 350 °C/100 min + 180 °C the maximum penetration depth of the MDEmax cavity decreases from 17.928 μm (for 1 h), at 15.128 μm (for 12 h), reaching 14.572 μm (for 24 h). After hardening the solution at 450 °C/100 min + 140 °C the maximum penetration depth of the MDEmax cavity decreases from 52.115 μm (for 1 h), at 43.017 μm (for 12 h), reaching 38.31 μm (for 24 h). After hardening the solution at 450 °C/100 min + 180 °C the maximum penetration depth of the MDEmax cavity decreases from 29.572 μm (for 1 h), at 29.471 μm (for 12 h), reaching 28.589 μm (for 24 h).
- After applying a solution hardening at 350 °C/100 min + artificial aging at 180 °C, the lowest penetration depths of the cavity are obtained both compared to the control

sample, with 60 μm, and compared to the samples subjected to hardening solution at 450 °C/100 min + artificial aging (either at 140 °C where the maximum depth of penetration is 38–52 μm, or at 180 °C, where the maximum penetration depth is about 29 μm).

- The best combination of heat treatments applied to cast aluminum products type 5083 is homogenization at 350 °C followed by artificial aging at 180 °C, at which the highest mechanical characteristics are obtained, a resilience of 25 J/cm^2, a grain size of 140–180 μm, and a maximum depth of the erosion MDEm around 14–17 μm.

Author Contributions: D.I.: conceptualization, methodology. B.-G.S.: X-rays diffraction analyses. A.M.D.: editing, data curation. A.D.B.: editing, data curation. L.S.: investigations. I.B.: methodology of cavitation, writing—original draft preparation. L.M.M.: cavitation experiments. C.G.: software, data curation. B.F.: methodology. B.G.: conceptualization, writing—original draft preparation, writing—reviewing and editing. All authors have read and agreed to the published version of the manuscript.

Funding: This research received no external funding.

Institutional Review Board Statement: Not applicable.

Informed Consent Statement: Not applicable.

Data Availability Statement: Not applicable.

Acknowledgments: This work has been funded by the European Social Fund from the Sectoral Operational Programme Human Capital 2014–2020, through the Financial Agreement with the title "Training of PhD students and postdoctoral researchers in order to acquire applied research skills—SMART", Contract no. 13530/16.06.2022—SMIS code: 153734.

Conflicts of Interest: The authors declare no conflict of interest.

References

1. Huang, K.; Lui, T.; Chen, L. Effect of microstructural feature on the tensile properties and vibration fracture resistance of friction stirred 5083 Alloy. *J. Alloys Compd.* **2011**, *509*, 7466–7472. [CrossRef]
2. Bauri, R.; Yadav, D.; Kumar, C.N.S.; Balaji, B. Tungsten particle reinforced Al 5083 composite with high strength and ductility. *Mater. Sci. Eng. A* **2015**, *620*, 67–75. [CrossRef]
3. Newbery, A.P.; Nutt, S.R.; Lavernia, E.J. Multi-scale Al 5083 for military vehicles with improved performance. *Jom-Us* **2006**, *58*, 56–61. [CrossRef]
4. Ke, W.; Bu, X.; Oliveira, J.; Xu, W.; Wang, Z.; Zeng, Z. Modeling and numerical study of keyhole-induced porosity formation in laser beam oscillating welding of 5A06 aluminum alloy. *Opt. Laser Technol* **2021**, *133*, 106540. [CrossRef]
5. Pereira, D.; Oliveira, J.; Santos, T.; Miranda, R.; Lourenço, F.; Gumpinger, J.; Bellarosa, R. Aluminium to Carbon Fibre Reinforced Polymer tubes joints produced by magnetic pulse welding. *Compos. Struct.* **2019**, *230*, 111512. [CrossRef]
6. Torzewski, J.; Grzelak, K.; Wachowski, M.; Kosturek, R. Microstructure and Low Cycle Fatigue Properties of AA5083 H111 Friction Stir Welded Joint. *Materials* **2020**, *13*, 2381. [CrossRef] [PubMed]
7. Tian, N.; Wang, G.; Zhou, Y.; Liu, K.; Zhao, G.; Zuo, L. Study of the Portevin-Le Chatelier (PLC) Characteristics of a 5083 Aluminum Alloy Sheet in Two Heat Treatment States. *States Mater.* **2018**, *11*, 1533. [CrossRef] [PubMed]
8. Nakamura, T.; Obikawa, T.; Nishizaki, I.; Enomoto, M.; Fang, Z. Friction Stir Welding of Non-Heat-Treatable High-Strength Alloy 5083-O. *Metals* **2018**, *8*, 208. [CrossRef]
9. Tamasgavabari, R.; Ebrahimi, A.; Abbasi, S.; Yazdipour, A. The effect of harmonic vibration with a frequency below the resonant range on the mechanical properties of AA-5083-H321 aluminum alloy GMAW welded parts. *Mater. Sci. Eng. A* **2018**, *736*, 248. [CrossRef]
10. Liu, Y.; Wang, W.; Xie, J.; Sun, S.; Wang, L.; Qian, Y.; Meng, Y.; Wei, Y. Microstructure and mechanical properties of aluminum 5083 weldments by gas tungsten arc and gas metal arc welding. *Mater. Sci. Eng.* **2012**, *549*, 7–13. [CrossRef]
11. Ma, M.; Lai, R.; Qin, J.; Wang, B.; Liu, H.; Yi, D. Effect of weld reinforcement on tensile and fatigue properties of 5083 aluminum metal inert gas (MIG) welded joint: Experiments and numerical simulations. *Int. J. Fatigue* **2021**, *144*, 106046. [CrossRef]
12. Corigliano, P.; Crupi, V.; Pei, X.; Dong, P. DIC-based structural strain approach for low-cycle fatigue assessment of AA 5083 welded joints. *Theor. Appl. Fract. Mech.* **2021**, *116*, 103090. [CrossRef]
13. Mânzână, M.E. Experimental Studies and Investigations Regarding the Structural Modifications Produced through Cavitation-erosion in Different Metallic Materials. Doctoral Thesis, University Politehnica of Bucharest, Bucharest, Romania, 2012.
14. Guragata, M.C. Studies and Experimental Researches Concerning Plastic Forming and Erosion-Cavitation Behavior of Superalloy Type INCONEL 718. PhD Thesis, University Politehnica of Bucharest, Bucharest, Romania, 2021.

15. Bordeașu, I. *Monograph of the Cavitation Erosion Research Laboratory of the University Politehnica of Timisoara (1960–2020)*; Politehnica Publishing House: Timisoara, Romania, 2020.
16. Micu, L.M. Cavitation Erosion Behavior of Duplex Stainless Steels. Doctoral Thesis, University Politehnica of Timisoara, Timisoara, Romania, 2017.
17. Bordeaşu, I.; Patrăşcoiu, C.; Bădărău, R.; Sucitu, L.; Popoviciu, M.O.; Bălăşoiu, V. New contributions to cavitation erosion curves modeling. *FME Trans.* **2006**, *34*, 39–43.
18. Cornelia Laura, S.; Bordeaşu, I.; Sîrbu, N.A.; Bădărău, R.; Mălaimare, G.; Hluscu, M.; Daniel, O.; Oancă, O.V. Evaluation of the Cavitation Resistance of INCONEL 718, in Delivered and Respectively Heat Treated Condition. *Adv. Mater. Res.* **2020**, *1157*, 47–51.
19. Istrate, D.; Ghera, C.; Sălcianu, L.; Bordeașu, I.; Ghiban, B.; Băzăvan, D.V.; Micu, L.M.; Stroiță, D.C.; Ostoia, D. Heat Treatment Influence of Alloy 5083 on Cavitational Erosion Resistance. *Hidraul. Mag.* **2021**, *3*, 15–25.
20. Bordeasu, I.; Mitelea, I. Cavitation Erosion Behavior of Stainless Steels with Constant Nickel and Variable Chromium Content. *Mater. Test.* **2012**, *54*, 53–58. [CrossRef]
21. *Standard G32*; Standard Method of Vibratory Cavitation Erosion Test. ASTM: West Conshohocken, PA, USA, 2016.
22. Mitelea, I.; Bordeaşu, I.; Riemschneider, E.; Uţu, I.D.; Crăciunescu, C.M. Cavitation erosion improvement following TIG surface-remelting of gray cast iron. *Wear* **2022**, *496*, 204282. [CrossRef]
23. Oanca Victor Octavian Techniques for Optimizing the Resistance to Cavitation Erosion of Some CuAlNiFeMn Alloys Intended for the Execution of Naval Propellers. Doctoral Thesis, University Politehnica of Timisoara, Timisoara, Romania, 2014.
24. Steller, K.; Reymann, Z.; Krzysztoowicz, T. Evaluation of the resistance of materials to cavitational erosion. In Proceedings of the Fifth Conference on Fluid Machinery, Akad Kiado, Budapest, 15–20 September 1975; Volume 2.
25. Sakai, I.; Shima, A. *On a New Representative Equation for Cavitation Damage Resistance of Materials*; Report, No. 385; Magazine of Hydraulics, Pneumatics, Tribology, Ecology, Sensorics, Mechatronics 24: Tokyo, Japan, 1987.
26. Micu, L.M.; Bordeasu, I.; Popoviciu, M.O. A New Model for the Equation Describing the Cavitation Mean Depth Erosion Rate Curve. *Chem. J.* **2017**, *4*, 894–898. [CrossRef]
27. Garcia, R. *Comprehensive Cavitation Damage Data for Water and Various Liquid Metals Including Correlation with Material and Fluid Properties*; Technical Report No. 6; University of Michigan: Ann Arbor, MI, USA, 1966.
28. Hobbs, J.M. Experience With a 20-kc Cavitation Erosion Test. In *Erosion by Cavitation or Impingement*; ASTM International: West Conshohocken, PA, USA, 1967; pp. 159–185.
29. Jean-Pierre, F.; Jean-Louis, K.; Karimi, A.; Fruman, D.-H.; Fréchou, D.; Briançon-Marjollet, L.; Billard, J.-Y.; Belahadji, B.; Avellan, F.; Michel, J.M. *Physical Mechanisms and Industrial Aspects*; Presses Universitaires de Grenoble: Grenoble, France, 1995.
30. Bordeasu, I.; Ghera, C.; Istrate, D.; Sălcianu, L.; Ghiban, B.; Băzăvan, D.V.; Micu, L.M.; Stroiţă, D.C.; Suta, A.; Tomoiagă, I. Resistance and Behavior to Cavitation Erosion of Semi-Finished Aluminum Alloy 5083. *Hidraul. Mag.* **2021**, *4*, 17–24.